Mechanism of Accelerated Assembly of β-Amyloid Filaments into Fibrils by $KLVFFK_6$

Jin Ryoun Kim and Regina M. Murphy
Department of Chemical and Biological Engineering, University of Wisconsin, Madison, Wisconsin

ABSTRACT Extracellular senile plaques are a central pathological feature of Alzheimer's disease. At the core of these plaques are fibrillar deposits of β-amyloid peptide (Aβ). In vitro, Aβ spontaneously assembles into amyloid fibrils of cross-β sheet structure. Although it was once believed that the fibrils themselves were toxic, more recent data supports the hypothesis that aggregation intermediates, rather than fully formed fibrils, are the most damaging to neuronal tissue. In previously published work, we identified several small peptides that interact with Aβ and increase its aggregation rate while decreasing its toxicity. In this work, we examined in detail the interaction between Aβ and one of these peptides. Using a mathematical model of Aβ aggregation kinetics, we show that the dominant effect of the peptide is to accelerate lateral association of Aβ filaments into fibrils.

INTRODUCTION

Alzheimer's disease (AD) is an age-associated neurodegenerative disease characterized by loss of memory and language skills, damaged cognitive function, and altered behavior. A central pathological feature of AD is the presence of extracellular senile plaques, found in the hippocampus and the neocortex and associated with synaptic loss and cell death (Selkoe, 1991). At the core of senile plaques are proteinaceous amyloid deposits. Chemical analysis of these deposits revealed that the major protein constituent is β-amyloid (Aβ) (Glenner and Wong, 1984; Masters et al., 1985). Aβ is a 39–43 residue proteolytic fragment of a larger integral membrane protein called amyloid precursor protein (APP) (Kang et al., 1987).

Aβ undergoes aggregation spontaneously and assembles into amyloid fibrils with a cross β-sheet structure (Kirschner et al., 1987). Aβ assembly can be accelerated by several factors, including locally high Aβ concentration, acidic pH, metal ions, osmolytes, and interaction with lipid membranes (Barrow and Zagorski, 1991; Hilbich et al., 1991; Fraser et al., 1992; Yang et al., 1999; Yip et al., 2002; for review see McLaurin et al., 2000). Electron microscopy (EM) studies demonstrated that Aβ fibrils from senile plaques are straight and unbranched, 5–12 nm in diameter, and appear to be in a helical array of β-sheet structure (Burkoth et al., 2000; for review see Serpell, 2000).

Multiple observations indicate that amyloid fibril formation is an early and required event in the AD neurodegenerative process (Pike et al., 1993; Selkoe, 1993; Simmons et al., 1994; Moran et al., 1995; Geula et al., 1998). The ''amyloid cascade'' hypothesis for AD postulates that amyloid fibril accumulation directly leads to synaptic loss, neuritic dystrophy, and the neurotransmitter deficits that are manifestations of dementia (Hardy and Higgins, 1992). However, more recent in vitro observations have demonstrated that small, soluble, and diffusible oligomeric Aβ species are also capable of initiating pathogenic events (Roher et al., 1996; Lambert et al., 1998; Hartley et al., 1999). These data have motivated several researchers to postulate that Aβ oligomeric intermediates, rather than fully formed fibrils, are the predominant toxic species (Kirkitadze et al., 2002).

Considerable research effort has focused on discovery of candidate compounds that block the toxicity of Aβ, by targeting a specific step involved in Aβ aggregation (Camilleri et al., 1994; Tomiyama et al., 1994; Klunk et al., 1998; Pappolla et al., 1998; Hughes et al., 2000). Given the hypothesis that aggregation intermediates are responsible for Aβ toxicity, such compounds could theoretically prevent all aggregation, or alternatively cause further association of toxic oligomers into larger nontoxic aggregates. In previous work from our group, a strategy for designing peptidyl inhibitors against Aβ toxicity was proposed (Pallitto et al., 1999; Lowe et al., 2001). Briefly, the inhibitors were envisioned as containing a ''recognition domain,'' a short peptide sequence homologous to a fragment of full-length Aβ (KLVFF, 16–20), and a ''disrupting domain,'' a polypeptide chain with the ability to interfere with Aβ aggregation. Inhibitors that protected PC-12 cells from Aβ toxicity actually increased the rate of Aβ aggregation (Pallitto et al., 1999; Lowe et al., 2001). Among these peptides, $KLVFFK_6$ was the most potent at preventing Aβ-associated toxicity to PC-12 cells and caused the largest change in Aβ aggregation kinetics and aggregate morphology (Pallitto et al., 1999).

In previous work, we developed a mathematical model of Aβ aggregation kinetics from in vitro experimental data (Pallitto and Murphy, 2001). In this article, we carefully evaluated Aβ aggregation kinetics in the presence of $KLVFFK_6$. Several questions we addressed include: 1), Does the inhibitor change the distribution of Aβ between nonamyloid and amyloid pathways? 2), Which specific step in the

Submitted November 14, 2003, and accepted for publication January 14, 2004.

Address reprint requests to Dr. Regina M. Murphy, Dept. of Chemical and Biological Engineering, University of Wisconsin, 1415 Engineering Dr., Madison, WI 53706. Tel: 608-262-1587; Fax: 608-262-5434; E-mail: murphy@che.wisc.edu.

0006-3495/04/05/3194/10 $2.00

Aβ aggregation pathway is the most affected by $KLVFFK_6$? 3), What is the mechanism of interaction between Aβ and inhibitors? To answer these questions, physicochemical measurements were collected and the data analyzed using the kinetic model.

MATERIALS AND METHODS

Peptide synthesis

Aβ(1–40) was purchased from AnaSpec (San Jose, CA). $KLVFFK_6$ was synthesized by solid phase peptide synthesis using Fmoc-protected amino acids and purified by reverse phase high-pressure liquid chromatography on a C4 column (Vydac, Hesperia, CA) using linear gradient of acetonitrile/water with 0.1% trifluoroacetic acid. Molecular mass of $KLVFFK_6$ was analyzed by mass spectrometry to be 1421.7 Da (theoretical molecular mass of 1421.9 Da). Peptides were stored as lyophilized powders at −70°C.

Sample preparation

Phosphate-buffered saline with azide ((PBSA) 0.01 M Na_2HPO_4/NaH_2PO_4, 0.15 M NaCl, 0.02% (w/v) NaN_3, pH 7.4) was double filtered through 0.22-μm filters. Urea (8 M) was prepared in 10 mM glycine-NaOH buffer, pH 10, then filtered through 0.22-μm filters. Lyophilized Aβ(1–40) was solubilized at a concentration of 2.8 mM using prefiltered 8 M urea, pH 10. After 10 min, samples were diluted to 140 μM Aβ into filtered PBSA, or PBSA containing $KLVFFK_6$. Samples were rapidly filtered through 0.45-μm filters directly into light-scattering cuvettes (for light scattering (LS)) or microtubes (for size exclusion chromatography (SEC)). Molecular-biology-grade urea was purchased from Boehringer-Mannheim (Indianapolis, IN). All other chemicals were purchased from Sigma-Aldrich (St. Louis, MO). The concentration of Aβ was determined from the peak area of the sample injected onto the fast protein liquid chromatography system without the column in place, using an extinction coefficient of 0.3062 $(mg/ml)^{-1}\ cm^{-1}$ (Pallitto and Murphy, 2001), and was 120 ± 20 μM. Residual urea was 0.4 M. Urea dissolution was required to yield highly quantitatively reproducible results and to ensure a controlled initial state. The urea may change absolute rates of aggregation, but does not change trends (Lowe et al., 2001).

Size exclusion chromatography

Samples were analyzed with SEC using a precision column prepacked with Superdex 75 (Pharmacia, Piscataway, NJ) on a Pharmacia fast protein liquid chromatography system, as described previously (Pallitto and Murphy, 2001). Briefly, the mobile phase flow rate was set at 0.05 ml/min and elution peaks were detected by ultraviolet (UV) absorbance at either 214 or 280 nm. Mobile phase buffer was matched to buffer used for dissolution of Aβ. The column was calibrated using the following proteins as molecular weight standards: insulin chain B (3500), ubiquitin (8500), ribonuclease A (13,700), ovalbumin (43,000), and bovine serum albumin (67,000). To determine the distribution between small oligomers that could be resolved on the column (molecular mass 3–70 kDa), and larger species that could not be resolved, samples were injected without the column in place; the percent of non-aggregates (monomer and dimer ($M+D$)) was calculated by dividing the $M+D$ peak area by the peak area without the column in place.

Laser light scattering

Samples prepared as described above were placed in a bath of the index-matching solvent decahydronaphthalene, which was temperature controlled to 25°C. Dynamic light scattering data were taken using a Coherent (Santa Clara, CA) argon ion laser operated at 488 nm and a Malvern 4700c system (Southborough, MA), as described in more detail elsewhere (Lowe et al., 2001).

Information on average particle molecular mass, shape, and dimensions were obtained using static light scattering measurements, as described previously in detail (Murphy and Pallitto, 2000). Two alternative models of particle shape, semiflexible (wormlike) chain and semiflexible branched, were used to fit the data. The semiflexible chain model describes a linear chain with total contour length L_c and Kuhn statistical segment length l_k (a measure of the stiffness of the chain, equal to two times the persistence length). We have shown previously that this model is a good description of Aβ fibrils (Shen et al., 1993; Shen and Murphy, 1995). The continuous semiflexible branched model describes a branched particle with a center from which extend n_b (number of branches) semiflexible chains of contour length $L_{c,a}$ and stiffness l_k.

Circular dichroism spectroscopy

Secondary structure of Aβ was determined using circular dichroism (CD), collected using an Aviv 62A DS circular spectrometer (Lakewood, NJ) in the far-UV range with 0.1 cm of pathlength of cuvette. Ellipticity of sample containing 140 μM of Aβ with and without addition of $KLVFFK_6$ at each wavelength was measured without dilution for 5 s and then averaged out. The lower wavelength boundary was limited to 211 nm due to the residual urea (0.4 M) in the sample. The spectrum of the background was measured for 5 s and averaged, followed by that of the sample. The average background was then subtracted from the average sample spectrum. The percent of each secondary structure element was calculated by nonlinear least square curve fitting of experimental ellipticities using several standard methods (Provencher and Glöckner, 1981; Manavalan and Johnson, 1987).

Mathematical modeling

A mathematical model of Aβ aggregation kinetics was developed by Pallitto and Murphy (2001). A schematic of the model is shown in Fig. 1. Diameters of filament and fibril were assumed to be 3 and 8 nm, respectively. Model equations were solved numerically, and parameter values were obtained by multiresponse nonlinear regression, as described previously (Pallitto and Murphy, 2001).

RESULTS

To allow for a more rigorous analysis of Aβ kinetics, 8 M urea/pH 10 was used to completely dissolve Aβ and render it monomeric and random coil before dilution into PBSA to initiate aggregation (Pallitto and Murphy, 2001). A mathematical model describing the kinetics of assembly was developed previously (Pallitto and Murphy, 2001). A schematic of the model is shown in Fig. 1. Briefly, denatured monomers M_u rapidly refolded into either stable monomer M or dimer D, or less stable dimeric intermediate I. I co-operatively assembled to nucleus N to initiate formation of thin filaments f. Filaments grew linearly by repeated addition of I. Cooperative lateral association of filaments resulted in formation of fibrils F. F elongated by end-to-end association. The kinetic model was in good agreement with SEC and LS experiments.

$KLVFFK_6$ protected PC-12 cells from Aβ-associated toxicity while significantly accelerating Aβ aggregation (Pallitto et al., 1999). In those experiments, Aβ was dissolved in 0.1% trifluoroacetic acid before dilution into PBSA

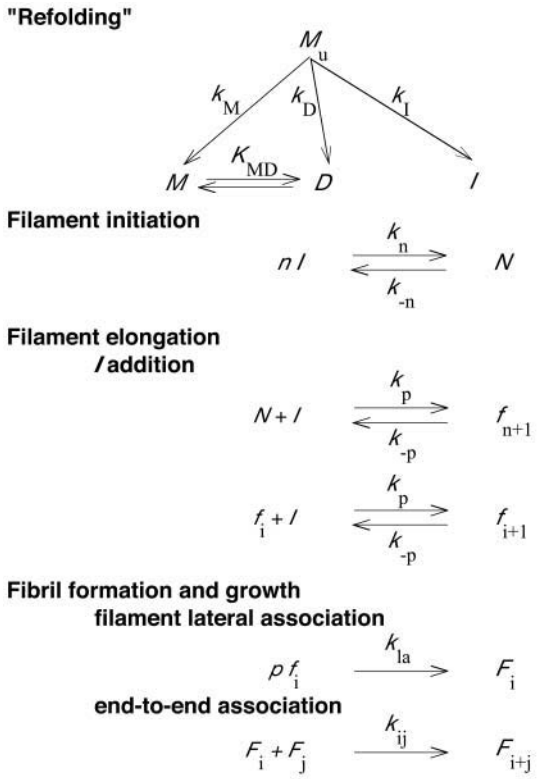

FIGURE 1 A schematic showing Aβ aggregation kinetic model (Pallitto and Murphy, 2001).

Model parameters	
K_{MD}	*M - D equilibrium* (μM^{-1})
k_M / k_I	*Relative rate of M to I formation from* M_u (μM)
k_D / k_I	*Relative rate of D to I formation from* M_u (–)
k_n / k_p	*Relative rate of filament initiation versus filament elongation* ($\mu M^{-5} h^{-1}$)
k_{la}	*Rate of lateral alignment of filaments* ($\mu M^{-2} h^{-1}$)
$\delta\omega_{fib}$	*Factor for base rate of end-to-end association of fibrils (cm-rad)*

containing test inhibitory peptide. In the work presented here, we used the mathematical model to evaluate the mechanism underlying the effect of $KLVFFK_6$ on aggregation kinetics of Aβ, starting from the urea-unfolded state. Points of interest include: a), alteration of secondary structure of Aβ; b), change in initial $M+D$ and I split; c), shift of Aβ nucleation/elongation balance; d), acceleration/deceleration of filament assembly to fibril; and e), extent of incorporation of $KLVFFK_6$ into Aβ.

Effect of $KLVFFK_6$ on Aβ secondary structure

Aβ aggregation is linked to conversion of the peptide from random coil to β-sheet secondary structure. Aβ in 8 M urea/pH 10 is random coil, but after dilution into PBSA, Aβ spontaneously aggregates into β-sheet fibrils. We evaluated whether $KLVFFK_6$ increased the extent of β-sheet structure. Circular dichroism spectra were taken on samples containing 140 μM Aβ and varying concentrations of $KLVFFK_6$ (0:1, 0.1:1, 0.5:1, and 1:1 $KLVFFK_6$:Aβ molar ratio). $KLVFFK_6$ alone was random coil (Fig. 2). $KLVFFK_6$ did not alter CD spectrum of Aβ at any concentration, indicating no disturbance of secondary structure by $KLVFFK_6$ (Fig. 2). Deconvolution of CD spectra revealed ~35% of β-sheet structure regardless of presence or absence of $KLVFFK_6$.

Effect of $KLVFFK_6$ on Aβ population

Dilution of Aβ from urea into PBSA produces a distribution of variously sized species. Under our experimental conditions, ~63% of total Aβ was present as stable Aβ monomer or dimer, whereas the remainder was aggregates of >70 kDa, consistent with previous reports (Pallitto and Murphy, 2001). Size exclusion chromatography experiments were performed to see whether $KLVFFK_6$ changed the distribution of Aβ species between nonamyloidogenic and

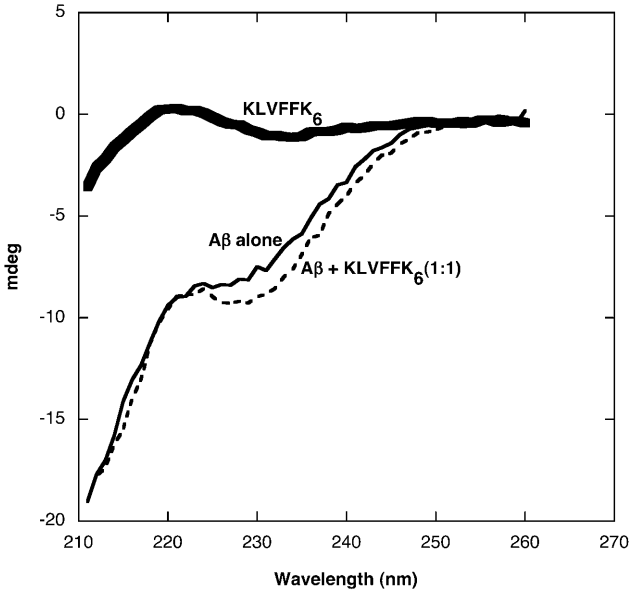

FIGURE 2 Circular dichroism (CD) spectra of 140 μM of $KLVFFK_6$ alone (*thick solid line*), Aβ alone (*thin solid line*), and $KLVFFK_6$ + Aβ at 1:1 (*dashed line*). Data for the other molar ratio of $KLVFFK_6$:Aβ we tested were indistinguishable from those for Aβ alone and 1:1 ratio of $KLVFFK_6$ + Aβ (data not shown). All samples contained 140 μM of Aβ and were incubated for ~18–20 h before CD measurements. For a given wavelength, data were collected for 5 s and averaged out. Due to residual urea, the minimum wavelength was limited to 211–212 nm.

amyloidogenic states. Detection was set at 280 nm, at which wavelength Aβ, but not $KLVFFK_6$, is detected. Percentages of Aβ monomer or dimer and aggregates were calculated and compared to Aβ alone (Table 1). Aβ population was not affected by $KLVFFK_6$, and the distribution did not change over time (data not shown).

Incorporation of $KLVFFK_6$ into Aβ

If $KLVFFK_6$ bound to Aβ monomers and dimers, one might expect a shift in elution time of the $M+D$ peak caused by a molecular mass increase. No such shift was observed in the presence of $KLVFFK_6$ (data not shown). This result indicates that $KLVFFK_6$ is not associated to any measurable extent with monomeric or dimeric Aβ species. We repeated SEC analysis of Aβ + $KLVFFK_6$ with detection at 214 nm, where both Aβ and $KLVFFK_6$ contributes to absorbance. We observed a significant peak at 39 min elution time, matching that of $KLVFFK_6$ alone (data not shown). Comparison of the area of this peak in the absence and presence of Aβ suggested most (>90%) of $KLVFFK_6$ eluted as free peptide, although accurate quantification was not possible due to low signal/noise ratio. This result implied very little of $KLVFFK_6$ is incorporated into aggregated Aβ.

TABLE 1 Effect of $KLVFFK_6$ on Aβ population

	Aβ alone*	$KLVFFK_6$ + A$\beta^{\dagger}$
% of aggregates (>70 kDa)‡	37 ± 8	38 ± 4
% of nonaggregates ($M + D$)‡	63 ± 8	62 ± 4

*Sample contained 140 μM of Aβ.

†Sample contained 140 μM of $KLVFFK_6$ and 140 μM of Aβ.

‡The identical samples were injected using the same sample loop and detector with and without the column in place. To calculate the fraction of Aβ in monomer and dimer populations, the individual peak areas (obtained with the column in place) were divided by the peak area without the column. The fraction of aggregates (>70 kDa) was calculated by difference. All values are mean ± SD of six independently prepared samples.

Effect of $KLVFFK_6$ on Aβ aggregation kinetics

We evaluated Aβ aggregation kinetics in the presence of varying concentrations of $KLVFFK_6$ using light scattering. Data are reported as average hydrodynamic diameter, d_{sph} and scattering intensity at 90° angle, $I_s(90°)$, versus time. Because small species contribute less to scattered light, d_{sph} and $I_s(90°)$ indicate primarily the change in size and/or mass of aggregates rather than of Aβ $M+D$. The rate of increase in d_{sph} and $I_s(90°)$ increased, with increasing amounts of $KLVFFK_6$. The increase in $I_s(90°)$ was approximately twofold greater than the increase in d_{sph} (Fig. 3). Because $I_s(90°)$ scales approximately with average aggregate molecular mass, whereas d_{sph} scales approximately with average aggregate length, these results indicate that $KLVFFK_6$ increased the linear density (mass per unit length) of Aβ aggregates.

Effect of $KLVFFK_6$ on Aβ aggregate size and shape

We wondered whether the morphology of Aβ aggregates changed in the presence of $KLVFFK_6$. To determine this, we collected static light scattering data at multiple angles; results are presented as a Kratky plot (Fig. 4). For Aβ alone and $KLVFFK_6$ + Aβ (1:1 molar ratio), the Kratky plots were fairly linear, characteristic of a rodlike morphology. With increasing concentration of $KLVFFK_6$, a shift of the aggregate morphology was apparent. At 2.5:1 molar ratio, a plateau at higher angles was observed, indicative of longer fibrils and a linear semiflexible chain morphology. At 5:1 and 10:1 molar ratio, there was a substantial change in the curve, exhibiting an intermediate ''bump'' that is characteristic of a branched morphology.

$\langle M\rangle_w$, L_c (or $L_{c,a}$), l_k, and n_b were determined by fitting the data to model equations for the appropriate particle structure function. Results are summarized in Table 2. Both $\langle M\rangle_w$ and L_c increased with increasing concentration of $KLVFFK_6$, with a greater increase in $\langle M\rangle_w$ than L_c. The increase in $\langle M\rangle_w/L_c$ implies greater average linear density with increasing concentration of $KLVFFK_6$, consistent with results shown in Fig. 3.

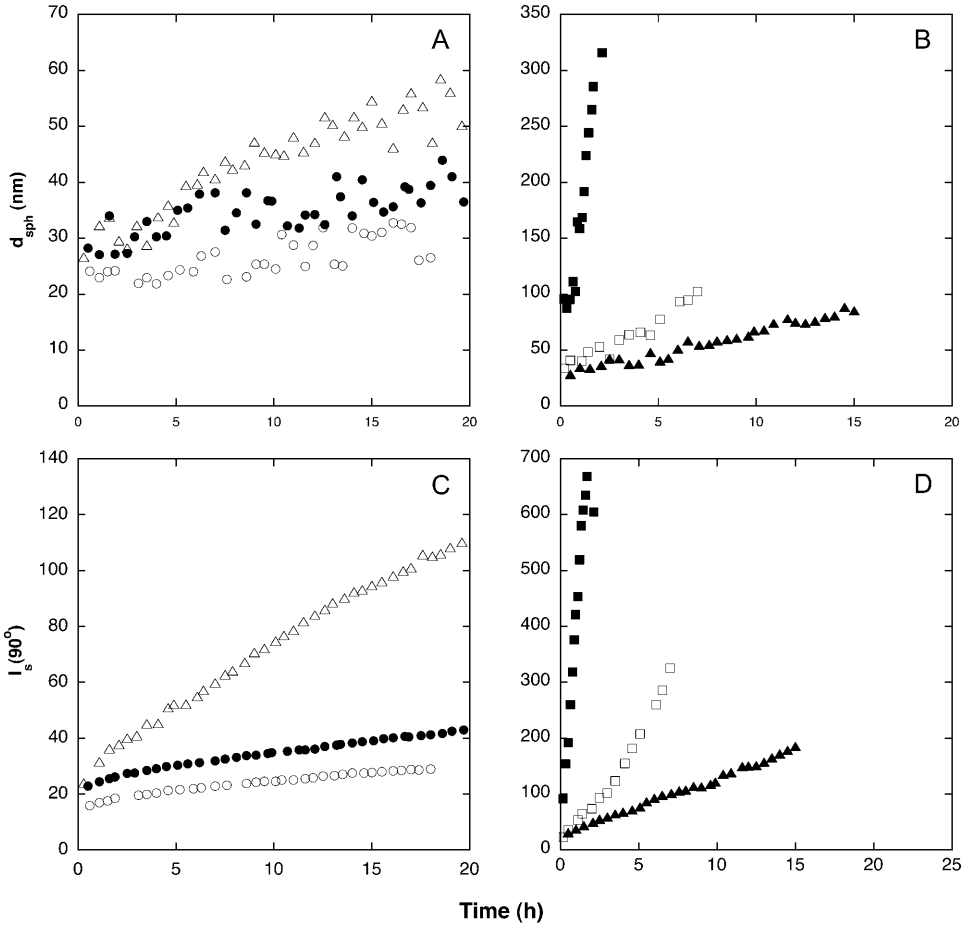

FIGURE 3 Hydrodynamic diameter d_{sph} (*A* and *B*) and scattering intensity at 90° angle $I_s(90°)$ (*C* and *D*) for Aβ alone (○), $KLVFFK_6$ + Aβ (1:10) (●), (1:1) (△), (2.5:1) (▲), (5:1) (□), and (10:1) (■). All samples contained 140 μM Aβ.

Kinetic model of Aβ aggregation in the presence of $KLVFFK_6$

Data were analyzed based on the kinetic model developed previously (Pallitto and Murphy, 2001). SEC and CD data indicated that $KLVFFK_6$ does not change the split between amyloidogenic and nonamyloidogenic Aβ, implying no change in the ''refolding'' step; this is reflected in the model as no change in K_{MD}, k_M/k_I, and k_D/k_I (Fig. 1). $KLVFFK_6$ did, however, strongly affect kinetics of growth in a concentration-dependent manner. Therefore, the major change is downstream of the ''refolding'' step (Fig. 1). Light scattering data were used to obtain the best fit parameter values for filament initiation and elongation (k_p/k_n), and fibril formation by lateral association (k_{la}) and fibril growth by end-to-end association ($\delta\omega_{fib}$) (Fig. 1). Because the kinetic model assumes a linear aggregate morphology, kinetic data of samples exhibiting a branched morphology could not be fitted to the model. For 5:1 ratio of $KLVFFK_6$:Aβ, it was not possible to obtain fits if the entire data set was used; therefore we used only data up to ~4 h to evaluate parameters. For the same reason, no attempt was made to fit any of the data for 10-fold excess of $KLVFFK_6$.

Our kinetic model captured growth of Aβ in the presence of $KLVFFK_6$ reasonably well (Fig. 5). Parameter values are summarized in Table 3. First, we examined the effect of $KLVFFK_6$ on filament initiation and elongation. k_n and k_p are rate constants governing nucleus *N* initiation from unstable intermediate species *I*, and filament initiation and growth by addition of *I*, respectively. Therefore, k_n/k_p represents the balance between new filament formation versus growth of existing filaments. k_n/k_p was not substantially affected by $KLVFFK_6$, indicating that the peptide did not disturb this balance. Then, we examined the effect of $KLVFFK_6$ on fibril formation and growth. k_{la} characterizes the rate of lateral association of filaments into fibrils, whereas $\delta\omega_{fib}$ characterizes the rate of growth by fibril end-to-end association. $\delta\omega_{fib}$ decreased moderately in the presence of $KLVFFK_6$. By far the greatest effect of $KLVFFK_6$ was on lateral association of filaments into fibrils: k_{la} increased by approximately fourfold at 1:10 ratio of $KLVFFK_6$:Aβ, ~70-fold at 1:1 ratio, and ~300-fold at 2.5:1 ratio.

DISCUSSION

Examination of the events by which monomeric Aβ associates into oligomers and fibrils is of central importance to elucidation of the molecular mechanisms underlying AD pathogenesis. The fact that fibrils formed in vitro are identical

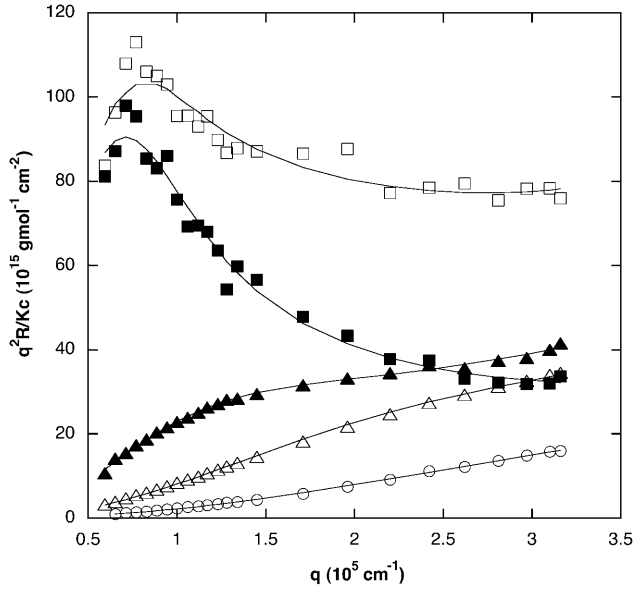

FIGURE 4 Effect of $KLVFFK_6$ on scattering intensity of Aβ aggregates. Data are presented in the form of Kratky plots. Data were collected 21 h after sample preparation for Aβ alone (○), $KLVFFK_6$ + Aβ (1:1) (△), (2.5:1) (▲), and (5:1) (□) or after 2 h for $KLVFFK_6$ + Aβ (10:1) (■). Each sample contained 140 μM Aβ. Lines indicate the fitted particle shape function, $P(q)$ for semiflexible chains (○, △, and ▲) or a branched structure (□ and ■). Kratky plot analysis of 10:1 sample after 21 h could not be made due to formation of significant amount of precipitates. c is the peptide concentration. $q = 4\pi n/\lambda_0 \sin(\theta/2)$, where n is the refractive index of the solvent, λ_0 is the wavelength of the incident beam in vacuo, and θ is the scattering angle. R is the Rayleigh ratio of sample. $K = 4\pi^2 n^2 (dn/dc)^2 / N_A \lambda_0^4$, where dn/dc is the refractive index increment, and N_A is Avogadro's number.

to those in vivo as determined by EM and x-ray diffraction, and are toxic to neuron cells, gives a strong justification for the validity of in vitro Aβ aggregation studies (Kirschner et al., 1987; Pike et al., 1993).

Peptides designed to interfere with Aβ aggregation also inhibited Aβ-associated toxicity (Pallitto et al., 1999; Lowe et al., 2001). Among these peptides, $KLVFFK_6$ was judged one of the most active. A detailed mathematical model of Aβ aggregation kinetics was previously proposed (Pallitto and Murphy, 2001), and we hypothesized that the model could be used to determine the specific step(s) in the aggregation pathway affected by $KLVFFK_6$.

We considered it possible that $KLVFFK_6$ could increase the Aβ aggregation rate by changing the secondary structure or the fraction of Aβ that is aggregated. However, analysis of CD spectra demonstrated that $KLVFFK_6$ did not change the β-sheet content of Aβ preparations. From SEC analysis, we observed no disturbance of the distribution of Aβ between M+D versus aggregated material. Furthermore, $KLVFFK_6$ does not appear to bind measurably to $M+D$ Aβ (data not shown). Together these results demonstrate that $KLVFFK_6$ does not act by associating with monomeric Aβ, by changing Aβ secondary structure, or by affecting the split of Aβ between nonamyloidogenic and amyloidogenic species (Fig. 1). Thus, its action is felt in a later step in the aggregation pathway.

Light-scattering analysis indicated that $KLVFFK_6$ does cause an increase in the rate of growth of aggregate size, as measured by both d_{sph} and $I_s(90°)$. The change in $I_s(90°)$ was greater than the change in d_{sph}, indicating that the increase in growth rate of the average molar mass of the aggregates was greater than the increase in growth rate of the average aggregate length. Closer analysis of the angular dependence of scattering showed that increasing the concentration of $KLVFFK_6$ increased the average molar mass and contour length of the aggregates, and led to changes in morphology from rigid rod to semiflexible chain to branched structures (Table 2 and Fig. 4). A greater mass per unit length in the presence of $KLVFFK_6$ was detected, consistent with observations from the fixed-angle scattering measurements.

The data were used to determine kinetic parameters in our model. Neither the balance between filament elongation versus initiation (k_p/k_n) nor end-to-end fibril growth ($\delta\omega_{fib}$) were affected much (Table 3). Rather, the major effect of $KLVFFK_6$ was to accelerate the rate of lateral association of filaments to fibrils, as evidenced by a large and dose-dependent increase in k_{la}. This finding is consistent with previous qualitative observations of an increase in linear

TABLE 2 Size characteristics of Aβ aggregates in the presence of $KLVFFK_6$

	Molar ratio ($KLVFFK_6$:Aβ)*				
	0:1†	1:1†	2.5:1†	5:1†	10:1‡
$\langle M\rangle_w$ (kDa)	190 ± 20	700 ± 20	4200 ± 200	57,000 ± 12,000	58,000 ± 9000
L_c (or $L_{c,a}$) (nm)	90 ± 5	160 ± 5	830 ± 30	1500 ± 500	1400 ± 400
l_k (nm)	ND§	ND§	200 ± 10	120 ± 50	130 ± 40
n_b	–	–	–	5 ± 2	9 ± 3

Data at the lowest three concentrations of $KLVFFK_6$ were analyzed using a linear semiflexible chain model, whereas at the highest two concentrations, the branched structure model was assumed. $\langle M\rangle_w$, weight-average molecular mass; L_c, the contour length of fibril in the semiflexible chain; $L_{c,a}$, the contour length of one arm in the branched structure; l_k, Kuhn statistical length; n_b, the number of branches in the branched structure.

*All samples contained 140 μM of Aβ.

†Data were taken 21 h after dilution.

‡Data were taken 2 h after dilution.

§ND, not determined. Because L_c is shorter than l_k, the fibrils behave as rigid rods and l_k cannot be determined.

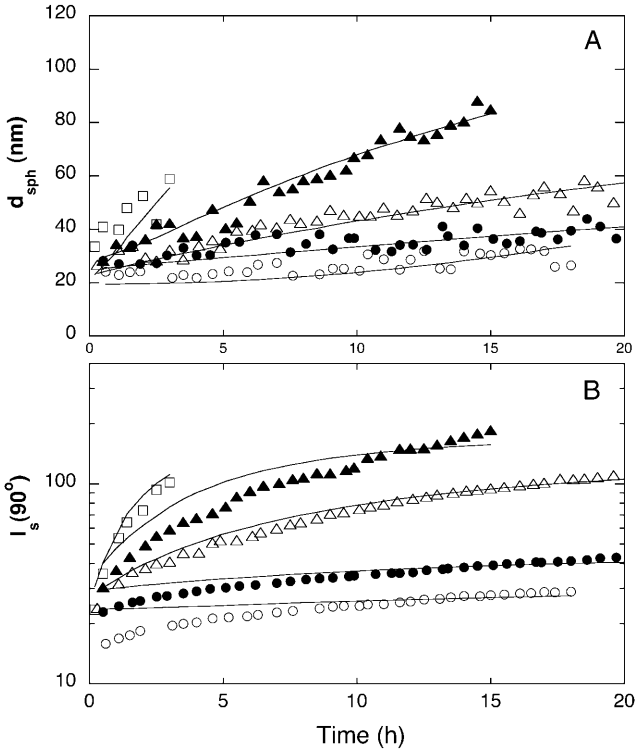

FIGURE 5 Measured average hydrodynamic diameter d_{sph} (*A*) and average scattering intensity $I_s(90°)$ (*B*) of Aβ aggregates for Aβ alone (○), KLVFFK$_6$ + Aβ (1:10) (●), (1:1) (△), (2.5:1) (▲), and (5:1) (□) are shown along with model simulations (*lines*) generated using parameters given in Table 3.

density of Aβ aggregates in the presence of KLVFFK$_6$ (Lowe et al., 2001; Moss et al., 2003).

We wondered whether we could interpret our results in light of recent findings about Aβ aggregate structure reported by the Tycko group (Tycko, 2003). Briefly, using solid-state NMR techniques, they proposed the following model: a), each Aβ molecule contains two β-strands (residues 13–24 and 30–40) separated by a bend (25–29); b), a double-layered ''cross-β unit'' is constructed from an Aβ dimer, with the two strands in each Aβ molecule belonging to separate β-sheets;

TABLE 3 Effect of KLVFFK$_6$ on model parameters

	Molar ratio (KLVFFK$_6$:Aβ)*				
	0:1	0.1:1	1:1	2.5:1	5:1
k_n/k_p (10^8 μM^{-5}h^{-1})	2.5 ± 2.0	9 ± 4	1.4 ± 0.5	0.7 ± 0.04	1.6 ± 0.9
k_{la} (10^3 μM^{-2}h^{-1})	0.3 ± 0.1	1.2 ± 0.3	20 ± 2	100 ± 20	160 ± 30
$\delta\omega_{fib}$† (10^8 cm-rad)	13 ± 6	7 ± 2	1.0 ± 0.1	1.6 ± 0.2	2.4 ± 0.8

Other parameters not shown here were set equal to previously determined values (Pallitto and Murphy, 2001).

*All samples contained 140 μM of Aβ.

†k_{ij} is calculated from $\delta\omega_{fib}$ as previously described (Pallitto and Murphy, 2001).

and c), a ''protofilament'' contains two cross-β units laterally assembled into a four-layered structure. The mass-per-unit length (MPL) of a single cross-β unit was estimated at 9 kDa/nm, and MPL of a protofilament at 18 kDa/nm. Protofilament formation is hypothesized to be driven by hydrophobic collapse occurring between the 30–40 strands in adjacent cross-β units. Further lateral association of protofilaments, via hydrophobic and electrostatic interactions, is allowed by the Tycko model. Atomic force microscopy studies from other groups provide further evidence of the existence of a mechanism for fibril growth by lateral association (Harper et al., 1997; Nichols et al., 2002).

We calculated MPL for our Aβ aggregates from $\langle M\rangle_w$, L_c, (Table 2) and the fraction of peptide that was aggregated (Table 1). Average MPL was estimated at ~6 kDa/nm for Aβ alone, and increased up to ~20 kDa/nm at high KLVFFK$_6$:Aβ ratio. These estimates are in the same range as those of Tycko (2003), and suggest that the aggregated species we observe are not highly laterally associated. In light of the Tycko model, we speculate that, at no or low KLVFFK$_6$, the detected species (what we call ''filaments'') are predominantly elongated cross-β units. As the KLVFFK$_6$ dose increases, there is a shift toward lateral assembly of cross-β units into ''protofilaments,'' and further alignment of ''protofilaments'' into fibrils. (Our model does not allow for a stable population of ''protofilaments''; their stability relative to elongated cross-β units and fibrils may depend on solvent conditions.) We propose that KLVFFK$_6$ increases the strength of the hydrophobic interaction, driving protofilament and fibril formation. We have recently reported on a chemical modification of KLVFFK$_6$ that increases solvent surface tension and greatly accelerates Aβ aggregation relative to KLVFFK$_6$ (Kim et al., 2003), in agreement with this hypothesis. This result, together with those reported here, is consistent with a speculation that this class of peptides drives Aβ aggregation via changes in solvent properties, therefore strengthening hydrophobically driven lateral association.

Despite the dramatic effect of KLVFFK$_6$ on lateral association, very little (<10%) of the peptide, if any, was actually incorporated into Aβ fibrils. Still, a peptide with a nonhomologous recognition element, KLVIIK$_6$, had no effect on Aβ aggregation (data not shown), indicating that some binding between KLVFFK$_6$ and Aβ must occur. We hypothesized that KLVFFK$_6$ binds reversibly to m binding sites on the filaments;

$$[f] + m[P] \leftrightarrow [f \cdot P_m], \tag{1}$$

where $[f]$ = free filament concentration, $[P]$ = free KLVFFK$_6$ peptide concentration, and $[f{\cdot}P_m]$ = filament-peptide complex concentration (all in μM). In the absence of KLVFFK$_6$, we modeled the kinetics of lateral association of filaments as a third-order process (Pallitto and Murphy, 2001):

$$\frac{d[F]}{dt} = k_{la}[f]^3. \quad (2)$$

Binding of $KLVFFK_6$ changes filament-filament versus filament-solvent energetics to favor filament-filament lateral association. In the presence of $KLVFFK_6$, we modeled lateral association of filaments with and without bound peptide also as a third-order process:

$$\frac{d[F']}{dt} = k'_{la}[f]^s[f \cdot P_m]^{3-s}, \quad (3)$$

where $0 \le s \le 3$, and F' is the fibrils formed in the presence of $KLVFFK_6$.

We hypothesized that:

$$k'_{la} \propto k_{la}\frac{[f \cdot P_m]^{3-s}[f]^s}{[f]^3},$$

or

$$\log k'_{la} = \text{constant} + \log k_{la} + (3-s)\log\left(\frac{[f \cdot P_m]}{[f]}\right), \quad (4)$$

where k_{la} is the lateral association rate constant for Aβ alone, and k'_{la} is the lateral association rate constant in the presence of $KLVFFK_6$ and is a function of the peptide's concentration and its affinity for binding to filaments. Because $[f]_{total} = [f] + [f{\cdot}P_m]$:

$$\log k'_{la} = \text{constant} + \log k_{la} + (3-s)\log\left(\frac{[f \cdot P_m]}{[f]_{total} - [f \cdot P_m]}\right), \quad (5)$$

where $[f]_{total}$ = total filament concentration (in μM). To evaluate these hypotheses, we need to determine how $[f{\cdot}P_m]$ changes with total peptide concentration. We assumed that $KLVFFK_6$ binds to m identical and noninteracting sites on Aβ filaments but does not bind to stable monomer or dimer, or,

$$\frac{[P_b]}{[f]_{total} \times m} = \frac{[P]}{[P] + K_d}, \quad (6)$$

where $[P_b]$ = concentration of peptide bound to filament. Because $[P_b]/m = [f \cdot P_m]$ on average and $[P] \approx [P]_{total}$ as described in Results, Eq. 5 is further reduced by combination with Eq. 6:

$$\log k'_{la} \approx \text{constant} + \log k_{la} + (3-s)\log\left(\frac{[P]_{total}}{K_d}\right). \quad (7)$$

We plotted $\log k'_{la}$ vs. $\log [P]_{total}$ from Table 3 and obtained a slope of $3 - s = 1.3$, or $s = 1.7$. Because $s < 3$, this analysis implies that only half of the filaments in a fibril must contain bound $KLVFFK_6$ to render significant change in lateral association. Using $K_d \sim 40$ μM for binding of $KLVFFK_6$ to Aβ (Cairo et al., 2002), combined with our observations that $<10\%$ of all $KLVFFK_6$ is bound to Aβ, and that the average filament is a 120-mer (Tables 1 and 2), we estimate from Eq. 6 that $m \approx 50$. Therefore $>60\%$ ((120 − 50)/120) of all Aβ molecules in a filament are protected, unable to bind to $KLVFFK_6$.

From our data, we were unable to ascertain whether $KLVFFK_6$ remained bound to fibrils (''stoichiometric'' mode) or was released from fibrils and available for another round of binding to filaments (''catalytic'' mode). Equation 7 suggests that stronger affinity (lower K_d) of peptide to Aβ leads to larger lateral association of filaments, as long as the amount of peptide bound to filament is small relative to total peptide concentration. In the catalytic mode, however, a very strong affinity of peptide binding to Aβ filaments would reduce the peptide's effectiveness at increasing lateral association. In other words, there would be an optimum binding affinity of peptide to Aβ, if these peptides act catalytically rather than stoichiometrically. With a panel of peptide inhibitors, lower K_d correlated strongly with greater effect on Aβ aggregation and greater potency in inhibiting toxicity (Cairo et al., 2002). However, in none of these peptides was the binding affinity strong enough to distinguish between catalytic and stoichiometric modes of action.

The fact that the predominant effect of $KLVFFK_6$ is to accelerate lateral alignment, leading to a decrease in the relative fraction of filament compared to fibril, is consistent with the hypothesis that intermediate species such as the cross-β unit or the protofilament are toxic (Kirkitadze et al., 2002). This is demonstrated in Fig. 6, where we use the kinetic model to calculate the filament and fibril fraction as a function of $KLVFFK_6$ concentration. Previous work from our group suggested that intermediate Aβ species with highly exposed hydrophobic patches interact most strongly with the lipid bilayer and lead to changes in membrane fluidity (Kremer et al., 2000). Such changes in membrane physical properties may produce harmful effects on cellular functioning. $KLVFFK_6$ could reduce Aβ toxicity by accelerating burial of these hydrophobic patches and driving formation of inert fully formed fibrils.

This analysis demonstrates the utility of a detailed mathematical model in interpreting the mode of action of putative aggregation modifiers. Specifically, for $KLVFFK_6$ we concluded that 1), this inhibitor does not change the distribution of Aβ between amyloid and nonamyloid paths; 2), this inhibitor affects most strongly the rate of lateral aggregation of Aβ filaments into fibrils; and 3), this inhibitor interacts with aggregated, not monomeric, Aβ, to enhance hydrophobically driven association. Such an analysis can contribute in two ways: first, to develop testable hypotheses for the mechanism of toxicity, and second, to suggest new design strategies in the search for better inhibitors of Aβ toxicity.

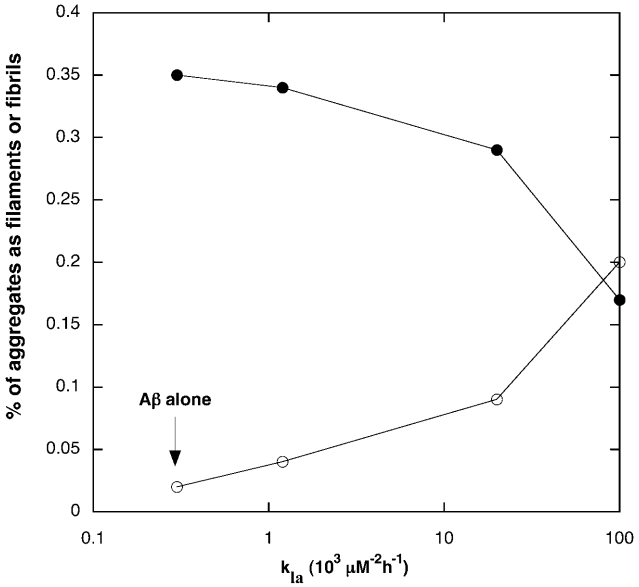

FIGURE 6 Weight fraction of filament (●) and fibril (○) simulated by the kinetic model using parameters given in Table 3. Points correspond to $KLVFFK_6$ + Aβ at (0:1), (0.1:1), (1:1), and (2.5:1) molar ratios.

We thank Todd Gibson for synthesizing $KLVFFK_6$.

This work was supported by National Institutes of Health grant AG 14079 from the National Institute of Aging. CD data were obtained at the University of Wisconsin-Madison Biophysics Instrumentation Facility, supported by NSF grants BIR-9512577 and S10RR13790, with help from Dr. Darrell McCaslin.

REFERENCES

Barrow, C. J., and M. G. Zagorski. 1991. Solution structures of β peptide and its constituent fragments: relation to amyloid deposition. *Science*. 253:179–182.

Burkoth, T. S., T. L. S. Benzinger, V. Urban, D. M. Morgan, D. M. Gregory, P. Thiyagarajan, R. E. Botto, S. C. Meredith, and D. G. Lynn. 2000. Structure of the β-amyloid (10–35) fibril. *J. Am. Chem. Soc.* 122:7883–7889.

Cairo, C. W., A. Strzelec, R. M. Murphy, and L. L. Kiessling. 2002. Affinity-based inhibition of β-amyloid toxicity. *Biochemistry*. 41:8620–8629.

Camilleri, P., N. J. Haskins, and D. R. Howlett. 1994. β-Cyclodextrin interacts with the Alzheimer amyloid β-A4 peptide. *FEBS Lett*. 341:256–258.

Fraser, P. E., J. T. Nguyen, D. T. Chin, and D. A. Kirschner. 1992. Effects of sulfate ions on Alzheimer β/A4 peptide assemblies: implications for amyloid fibril-proteoglycan interactions. *J. Neurochem*. 59:1531–1540.

Geula, C., C. K. Wu, D. Saroff, A. Lorenzo, M. Yuan, and B. A. Yankner. 1998. Aging renders the brain vulnerable to amyloid β-protein neurotoxicity. *Nat. Med*. 4:827–831.

Glenner, G. G., and C. W. Wong. 1984. Alzheimer's disease: initial report of the purification and characterization of a novel cerebrovascular amyloid protein. *Biochem. Biophys. Res. Commun*. 120:885–890.

Hardy, J. A., and G. A. Higgins. 1992. Alzheimer's disease: the amyloid cascade hypothesis. *Science*. 256:184–185.

Harper, J. D., C. M. Lieber, and P. T. Lansbury, Jr. 1997. Atomic force microscopic imaging of seeded fibril formation and fibril branching by the Alzheimer's disease amyloid-β protein. *Chem. Biol*. 4:951–959.

Hartley, D. M., D. M. Walsh, C. P. Ye, T. Diehl, S. Vasquez, P. M. Vassilev, D. B. Teplow, and D. J. Selkoe. 1999. Protofibrillar intermediates of amyloid β-protein induce acute electrophysiological changes and progressive neurotoxicity in cortical neurons. *J. Neurosci*. 19:8876–8884.

Hilbich, C., B. Kisters-Woike, J. Reed, C. L. Masters, and K. Beyreuther. 1991. Aggregation and secondary structure of synthetic amyloid βA4 peptides of Alzheimer's disease. *J. Mol. Biol*. 218:149–163.

Hughes, E., R. M. Burke, and A. J. Doig. 2000. Inhibition of toxicity in the β-amyloid peptide fragment β-(25–35) using N-methylated derivatives: a general strategy to prevent amyloid formation. *J. Biol. Chem*. 275: 25109–25115.

Kang, J., H. G. Lemaire, A. Unterbeck, J. M. Salbaum, C. L. Masters, K. H. Grzeschik, G. Multhaup, K. Beyreuther, and B. Muller-Hill. 1987. The precursor of Alzheimer's disease amyloid A4 protein resembles a cell-surface receptor. *Nature*. 325:733–736.

Kim, J. R., T. J. Gibson, and R. M. Murphy. 2003. Targeted control of kinetics of β-amyloid self-association by surface tension-modifying peptides. *J. Biol. Chem*. 278:40730–40735.

Kirkitadze, M. D., G. Bitan, and D. B. Teplow. 2002. Paradigm shifts in Alzheimer's disease and other neurodegenerative disorders: the emerging role of oligomeric assemblies. *J. Neurosci. Res*. 69:567–577.

Kirschner, D. A., H. Inouye, L. K. Duffy, A. Sinclair, M. Lind, and D. J. Selkoe. 1987. Synthetic peptide homologous to β protein from Alzheimer disease forms amyloid-like fibrils in vitro. *Proc. Natl. Acad. Sci. USA*. 84:6953–6957.

Klunk, W. E., M. L. Debnath, A. M. Koros, and J. W. Pettegrew. 1998. Chrysamine-G, a lipophilic analogue of Congo red, inhibits Aβ-induced toxicity in PC12 cells. *Life Sci*. 63:1807–1814.

Kremer, J. J., M. M. Pallitto, D. J. Sklansky, and R. M. Murphy. 2000. Correlation of β-amyloid aggregate size and hydrophobicity with decreased bilayer fluidity of model membranes. *Biochemistry*. 39:10309–10318.

Lambert, M. P., A. K. Barlow, B. A. Chromy, C. Edwards, R. Freed, M. Liosatos, T. E. Morgan, I. Rozovsky, B. Trommer, K. L. Viola, P. Wals, C. Zhang, C. E. Finch, G. A. Krafft, and W. L. Klein. 1998. Diffusible, nonfibrillar ligands derived from Aβ1–42 are potent central nervous system neurotoxins. *Proc. Natl. Acad. Sci. USA*. 95:6448–6453.

Lowe, T. L., A. Strzelec, L. L. Kiessling, and R. M. Murphy. 2001. Structure-function relationships for inhibitors of β-amyloid toxicity containing the recognition sequence KLVFF. *Biochemistry*. 40:7882–7889.

Manavalan, P., and W. C. Johnson. 1987. Variable selection method improves the prediction of protein secondary structure from circular-dichroism spectra. *Anal. Biochem*. 167:76–85.

Masters, C. L., G. Simms, N. A. Weinman, G. Multhaup, B. L. McDonald, and K. Beyreuther. 1985. Amyloid plaque core proteins in Alzheimer disease and Down syndrome. *Proc. Natl. Acad. Sci. USA*. 82:4245–4249.

McLaurin, J., D.-S. Yang, C. M. Yip, and P. E. Fraser. 2000. Review: modulating factors in amlyoid-β fibril formation. *J. Struct. Biol*. 130:259–270.

Moran, P. M., L. S. Higgins, B. Cordell, and P. C. Moser. 1995. Age-related learning deficits in transgenic mice expressing the 751-amino acid isoform of human β-amyloid precursor protein. *Proc. Natl. Acad. Sci. USA*. 92:5341–5345.

Moss, M. A., M. R. Nichols, D. K. Reed, J. H. Hoh, and T. L. Rosenberry. 2003. The peptide KLVFF-K(6) promotes β-amyloid(1–40) protofibril growth by association but does not alter protofibril effects on cellular reduction of 3-(4,5-dimethylthiazol-2-yl)-2,5-diphenyltetrazolium bromide (MTT). *Mol. Pharmacol*. 64:1160–1168.

Murphy, R. M., and M. M. Pallitto. 2000. Probing the kinetics of β-amyloid self-association. *J. Struct. Biol*. 130:109–122.

Nichols, M. R., M. A. Moss, D. K. Reed, W. L. Lin, R. Mukhopadhyay, J. H. Hoh, and T. L. Rosenberry. 2002. Growth of β-amyloid(1–40) protofibrils by monomer elongation and lateral association. Characterization of distinct products by light scattering and atomic force microscopy. *Biochemistry*. 41:6115–6127.

Pallitto, M. M., J. Ghanta, P. Heinzelman, L. L. Kiessling, and R. M. Murphy. 1999. Recognition sequence design for peptidyl modulators of β-amyloid aggregation and toxicity. *Biochemistry.* 38:3570–3578.

Pallitto, M. M., and R. M. Murphy. 2001. A mathematical model of the kinetics of β-amyloid fibril growth from the denatured state. *Biophys. J.* 81:1805–1822. (Errata published in *Biophys. J.* 82:2826.)

Pappolla, M., P. Bozner, C. Soto, H. Shao, N. K. Robakis, M. Zagorski, B. Frangione, and J. Ghiso. 1998. Inhibition of Alzheimer β-fibrillogenesis by melatonin. *J. Biol. Chem.* 273:7185–7188.

Pike, C. J., D. Burdick, A. J. Walencewicz, C. G. Glabe, and C. W. Cotman. 1993. Neurodegeneration induced by β-amyloid peptides in vitro: the role of peptide assembly state. *J. Neurosci.* 13:1676–1687.

Provencher, S. W., and J. Glöckner. 1981. Estimation of globular protein secondary structure from circular dichroism. *Biochemistry.* 20:33–37.

Roher, A. E., M. O. Chaney, Y. M. Kuo, S. D. Webster, W. B. Stine, L. J. Haverkamp, A. S. Woods, R. J. Cotter, J. M. Tuohy, G. A. Krafft, B. S. Bonnel, and M. R. Emmerling. 1996. Morphology and toxicity of Aβ-(1–42) dimer derived from neuritic and vascular amyloid deposits of Alzheimer's disease. *J. Biol. Chem.* 271:20631–20635.

Selkoe, D. J. 1991. The molecular pathology of Alzheimer's disease. *Neuron.* 6:487–498.

Selkoe, D. J. 1993. Physiological production of the β-amyloid protein and the mechanism of Alzheimer's disease. *Trends Neurosci.* 16:403–409.

Serpell, L. C. 2000. Alzheimer's amyloid fibrils: structure and assembly. *Biochim. Biophys. Acta.* 1502:16–30.

Shen, C. L., G. L. Scott, F. Merchant, and R. M. Murphy. 1993. Light scattering analysis of fibril growth from the amino-terminal fragment β(1–28) of β-amyloid peptide. *Biophys. J.* 65:2383–2395.

Shen, C. L., and R. M. Murphy. 1995. Solvent effects on self-assembly of β-amyloid peptide. *Biophys. J.* 69:640–651.

Simmons, L. K., P. C. May, K. J. Tomaselli, R. E. Rydel, K. S. Fuson, E. F. Brigham, S. Wright, I. Lieberburg, G. W. Becker, D. N. Brems, and W. Y. Li. 1994. Secondary structure of amyloid β peptide correlates with neurotoxic activity in vitro. *Mol. Pharmacol.* 45:373–379.

Tomiyama, T., S. Asano, Y. Suwa, T. Morita, K. Kataoka, H. Mori, and N. Endo. 1994. Rifampicin prevents the aggregation and neurotoxicity of amyloid β protein in vitro. *Biochem. Biophys. Res. Commun.* 204: 76–83.

Tycko, R. 2003. Insights into the amyloid folding problem from solid-state NMR. *Biochemistry.* 42:3151–3159.

Yang, D.-S., C. M. Yip, T. H. Huang, A. Chakrabartty, and P. E. Fraser. 1999. Manipulating the amyloid-β aggregation pathway with chemical chaperones. *J. Biol. Chem.* 274:32970–32974.

Yip, C. M., A. A. Darabie, and J. McLaurin. 2002. Aβ 42-peptide assembly on lipid bilayers. *J. Mol. Biol.* 318:97–107.